Journal of Atmospheric and Terrestrial Physics, Vol. 49, Nos. 7/8, pp. 621–637, 1987.
Printed in Great Britain.

0021–9169/87 $3.00 + .00
Pergamon Journals Ltd.

Large scale structure of the stratosphere and the lower mesosphere (20–60 km) over the northern hemisphere during the MAP/WINE campaign

K. PETZOLDT, R. LENSCHOW
Meteorological Institute, Free University of Berlin, F.R.G.

A. HAUCHECORNE
Service D'Aeronomy du CNRS, France

G. A. KOKIN
Central Aerological Observatory, Moscow, U.S.S.R.

W. MEYER
Physics Institute, University of Bonn, F.R.G.

A. O'NEILL
Meteorological Office, Bracknell, U.K.

C. R. PHILBRICK
Air Force Geophysics Laboratory, Hanscom Air Force Base, U.S.A.

F. SCHMIDLIN
NASA Goddard Space Flight Center, Wallops Island, U.S.A.

and

R. THOMAS
LASP, Boulder, Colorado, U.S.A.

(*Received for publication* 14 *January* 1987)

Abstract—All available temperature and wind measurements from radiosondes, rockets, satellites and lidar over the northern hemisphere have been used to construct large scale patterns of the temperature and circulation fields up to 60 km during the period 1 December 1983 to 1 March 1984. Main sources of information for the height range above 30 km are the uppermost spectral channel of the Stratospheric Sounding Unit (SSU) on-board the NOAA satellites and the meteorological rocket soundings. Rocket launches are generally scheduled on a weekly basis over the northern hemisphere, and the large scale patterns were derived for those days on which these measurements are available.

The method used to retrieve temperature fields from the satellite measured radiances contains several steps.

(a) First, estimated fields for the temperature at 7 pressure levels were constructed; in the lower middle stratosphere 50, 30 and 10 mbar level analyses by the stratospheric group Berlin were taken; at 5, 1, 0.4 and 0.2 mbar regressed temperature fields from the SSU radiances were updated by all *in situ* temperature measurements (the multiple regression coefficients have been derived for the period of MAP/WINE).

(b) Stratopause *height* fields were estimated by means of the temperature profiles provided by the Solar Mesosphere Explorer (SME) and rocket soundings. (c) With the input of (a) and (b) and the *a priori* assumption that the temperature maximum is situated at the stratopause height, a solution of the radiation transfer equation is possible for the measured SSU radiances with a time and space dependent stratopause.

The computed temperature fields are added hydrostatically to the 10 mbar height analysis, so that geopotential heights, geostrophic winds and temperatures at pressure levels up to 60 km become available once a week for dynamical computations.

The circulation will be described in terms of planetary waves and zonal means. The interaction of the waves with the mean flow, resulting in a breakdown of the westerly circulation at the end of February, will be discussed.

The remarkable changes at high latitudes over northern Europe are shown to be connected with processes at middle and low latitudes.

1. INTRODUCTION

The experiments of the MAP/WINE campaign were launched for different atmospheric conditions to obtain a large variety of the measured parameters. To specify these conditions it seems necessary to know not only the local atmospheric state, but also large scale motions forced by planetary waves and the mean circulation.

Whereas the local meteorological parameters were given by rockets launched frequently over Andøya, Norway, and Heiss Island, U.S.S.R., the northern hemispheric temperature fields could be taken from satellite observations. The SSU (NASH and BROWNSCOMBE, 1983) on-board the NOAA satellites and the SME (RUSH *et al.*, 1983) provided temperature information up to about 60 km. However, the commonly used statistical method for retrieving temperatures from radiances measured by the few stratospheric channels of satellite instruments are not convenient for disturbed conditions. This can clearly be shown by comparison of those temperature solutions with *in situ* measurements. Systematic errors would make subsequent dynamical computations meaningless. Therefore, a method for the temperature retrieval was used which gives a solution of the radiances from the SSU by fitting all *in situ* measurements taken in the stratosphere and mesosphere over the northern hemisphere, including some temperature information of the SME.

The difficulties and the approach of this method are illustrated in Section 2, to show how far a temperature analysis can be successful in the height range investigated by means of the available data source.

Further, in Section 3 the main features of the derived temperature and height fields are discussed during the winter, whereas in Section 4 the development of the dynamics are described in fluctuations of the zonal mean and planetary waves.

In Section 5 an attempt is made to realize how these fluctuations in the stratosphere and mesosphere are connected, with respect to their behaviour at low and high latitudes. The predominant ideas and open questions for the occurrence of a major warming are discussed.

2. DATA SOURCES AND APPLIED METHODS

Up to 30 km radiosondes are available, so that geopotential height and temperature fields can be analysed daily for the pressure levels 50, 30 and 10 mbar. In the upper stratosphere and lower mesosphere SSU radiances, SME temperature profiles, lidar observations and rocket measurements were used as temperature information. However, analyses of temperature fields over the whole northern hemisphere are not possible with only one of these sources. The few rocket stations do not provide enough horizontal coverage, while the three stratospheric channels of the SSU have insufficient vertical resolution for an analysis of disturbed temperature fields without additional information. The computation of temperatures from Rayleigh scattered sunlight by spectrometer measurements of the SME satellite is somewhat biased by aerosol scattering in the middle stratosphere, therefore it would be difficult to use these values for a temperature analysis. To overcome these problems a method was applied, where the retrieval of the SSU radiances yields temperatures which are nearest to first guesses taken from all information of 4 mandatory level temperatures (5, 1, 0.4 and 0.2 mbar) and a stratopause height (PETZOLDT, 1979).

The procedure starts with the statistical method usually applied to obtain temperature fields from statistically derived multiple regression coefficients (estimated by means of rocket temperatures and simultaneously measured satellite radiances). The regression coefficients for the MAP/WINE winter have been improved by using not only SSU radiances, but also the analysis of 10 mbar radiosonde temperatures. The computed correlation coefficients between upper level temperatures and 4 independent variables (10 mbar temperature, radiance of SSU channels 26 and 27 and the product of these radiances) are shown in Table 1 for rocket measurements during the period of MAP/WINE. U.S. metrockets show a stronger correlation than the U.S.S.R. rocket soundings, which might be due to the geographical location (more launching sites of U.S. rockets are at lower latitudes and thus are not so strongly affected by disturbances as those at higher latitudes).

Temperature differences between the rocket measurements of the U.S.A. and the U.S.S.R. are known from comparison of the LIMS sounder flown on-board the Nimbus 7 satellite in 1979 (GILLE *et al.*, 1984) and from rocket comparisons at Wallops Island and Kourou Space Centre (LEVITON, 1975). These systematic differences between both types of rocket instruments can also be seen by comparison of computed and observed radiances for channel 27 (max weight around 1.7 mbar) in Fig. 1. The plotted regression curves are computed separately for all U.S. (including Andøya) and all U.S.S.R. rockets. Forty-eight U.S. datasondes, including 26 rocket soundings at Andøya, (r.m.s. = 2.69 for the residuals of the regression curve) and 40 U.S.S.R. rocketsondes (r.m.s. = 2.64 for the residuals of the regression curve)

Table 1. Regression and correlation coefficients for multiple regression between rocketsonde temperatures A_i (at 4 mandatory levels) and independent variables B_j (satellite radiances, radiosonde analyses at 10 mbar)

Variables		Correlation coefficients	
Dependent	Independent U.S. regression coefficients (a, b_1, b_2, b_3, b_4)	U.S.	U.S.S.R.
T (5 mbar)	SSU 26, 27, 26*27, T (10 mbar) (−26.2, −0.266, −0.295, 0.0114, 0.47)	0.95	0.87
T (1 mbar)	SSU 26, 27, 26*27, T (10 mbar) (−141.3, 0.039, 2.452, −0.0107, 0.005)	0.87	0.83
T (0.4 mbar)	SSU 26, 27, 26*26, T (10 mbar) (19.3, −2.62, 1.197, 0.0103, 0.19)	0.74	0.71
T (0.2 mbar)	SSU 26, 27, 26*27, T (10 mbar) (24.9, 2.67, 0.656, 0.0012, −0.06)	0.78	0.70

A in °C; B in mW (m^2 ster cm^{-1})$^{-1}$ and °C

$$A_i = a_i + \sum_{j=1}^{4} b_{ij} B_j.$$

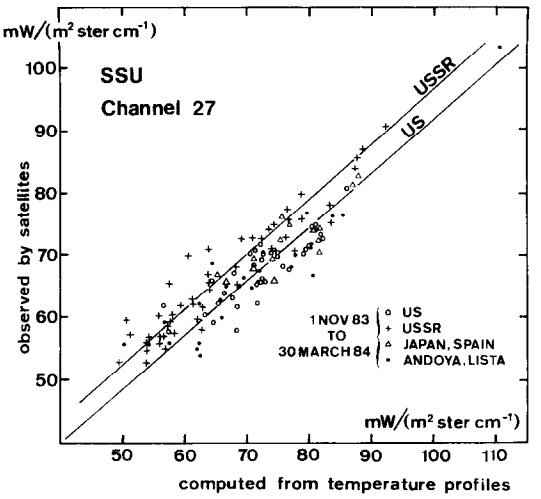

Fig. 1. Computed radiances from rocket measurements during the winter 1983/1984 compared with the observed radiances of SSU channel 27.

were utilized where satellite data were available during the period 1 December to 29 February 1984. The standard deviations are due to time and space differences between coordinated measurements, because observed radiance values of the daily SSU analyses are linearly interpolated to the time of the rocket sounding at the location of the rocket site. The systematic distance between the regression curves for U.S. and U.S.S.R. soundings corresponds to a mean temperature difference of about 5°, instead of more than 10° difference in the LIMS comparison for the domain of the weighting function of SSU channel 27. Whether there had been a change in the temperature sounding system of the U.S.S.R. rockets since 1979 is not known. Hemispherically analysed temperatures measured by rockets should be adjusted with these values to avoid biased differences between the eastern and the western part of the northern hemisphere. Because of the fact that in this investigation the regression coefficients of the U.S. rockets (Table 1) were taken for the first guess temperature fields and the retrievals were made from observed radiances adjusted to computed radiances for U.S. rocket soundings, the result are temperature profiles which would have been measured by the U.S. rocket sounder.

The next step is to improve these regressed first guess fields by means of all available *in situ* measurements of thermal wind and temperature. The decreasing correlation coefficients in Table 1 display very clearly that, especially for the upper levels, deviations should be expected between the regressed temperature values and the measured rocket temperatures. These are caused by real fluctuations (not distinguishable by the low weighted spectral satellite channels at those heights) and not by noise in the rocket soundings. The large scale temperature structure of the first guess fields had to be changed, therefore, to give agreement with the *in situ* measurements for each day analysed.

The difference between the computed radiance of the linear temperature profiles from those improved first guess fields and the observed radiance is assumed to have its origin in the stratopause region. Then for an exact temperature solution the *height* of the stratopause is needed. The temperature information of the SME satellite is used to give a stratopause

height for each measured orbital temperature profile. Though the temperatures themselves are biased in some layers by aerosols (too cold), the temperature maximum at the stratopause is well defined. A hemispheric stratopause height analysis (including all rocket measured stratopause heights) is therefore possible.

With the assumption that the temperature profile to be retrieved out of the radiances is linear (or another function) in $\ln(p)$ between the mandatory levels and also between the stratopause and the neighbouring mandatory levels, a solution of the radiation equation is possible, which in turn yields the temperature at the stratopause (PETZOLDT, 1980). Unrealistic lapse rates or unsolvable stratopause heights were prevented by iteratively changing first guess fields. This computer procedure was practised for each gridpoint in a 5° distance geographical grid.

As the SSU radiance analysis is a combination of all orbit values during one day, the large scale analysis should be understood as a 24 h mean state of the atmosphere. Therefore, no tidal component is included in the analyses, nor are the measurements tidally corrected. Also, the temperature solution, taken to be linear in $\ln(p)$ between the mandatory levels and between the stratopause and next mandatory level, does not include small vertical waves. Deviations which should be expected between the published analysis and *in situ* observations are illustrated at the maximum of the stratospheric warming in Fig. 6.

3. EVOLUTION OF THE WINTER VORTEX WITH MINOR AND MAJOR WARMINGS

The computed temperature and height fields on hemispheric maps at 10 mbar (28–30 km) and 0.2 mbar (55–60 km) give an impression of the development of the polar vortex during the MAP/WINE period up to the mesosphere (Fig. 2a, b).

At the beginning, on 1 December 1983, a Canadian warming in the Stratosphere had displaced the polar vortex to the Siberian arctic. Above the cold air in the vortex a very high stratopause with temperatures about 0°C was observed near Andøya, Norway. The stratopause was sloping below the 0.2 mbar level in all other regions (Figs. 3b and 5b), so that the warm polar area means a weakening vortex in the upper mesosphere.

Further cooling in the stratosphere strengthened the vortex during December, while the vortex center shifted westward over Spitzbergen towards Greenland. This marked the beginning of the cold midwinter season. The warmest area at 0.2 mbar remained over the European arctic.

Planetary wave activity increased again during the second half of December (LABITZKE *et al.*, 1984) at high latitudes in the upper stratosphere. Connected with this process is a sinking stratopause and a temperature decrease in the mesosphere—detectable by temperatures of −50°C at 0.2 mbar. This stratospheric warming in the eastern part of the northern hemisphere coupled with a cooling in mesospheric heights also affected the area over northern Europe as seen in the time/height section over Andøya of OFFERMANN *et al.* (1987).

During January the polar vortex recovered and at the end of this month the minimum temperature in the stratosphere was reached (−90°C near 19 km at 50 mbar), causing a very deep vortex at 10 mbar centered at the north pole. At 0.2 mbar the temperature shows a relatively disturbed structure. Fast temperature changes, as observed over Andøya, Norway, at that time, seem to be related to these wave-like disturbances.

Until 9 February a strong Aleutian anticyclone had developed in the stratosphere and again the vortex was shifted towards the European arctic. The stratopause evolved dramatically after that time, as shown in Fig. 2b.

In the southwesterly jetstream between the stratospheric anticyclone and the vortex a patch of warm air is sloping northwestward with height on 16 February. The stratopause temperature achieved a maximum at 0.2 mbar in polar regions. During the following week the temperature at the sinking stratopause increased further; highest temperature values (near 35°C) were computed from SSU radiances on 23 February between 65° and 70°N around 3 mbar at 30°E.

4. SYNOPSIS OF THE ZONAL MEAN STATE AND THE PLANETARY WAVES

To get some insight into the dynamical evolution within the winter period, it seems worth following the development of the mean zonal wind maximum and the amplitudes of the largest planetary waves. As is known, the shear of mean flow plays a leading role in linear wave theory for the refraction of planetary waves (MATSUNO, 1970), which are themselves mainly responsible for the transport of momentum and sensible heat.

4.1. *Zonal mean state*

Three episodes can be distinguished having a mean period of one month. Each of them is terminated by

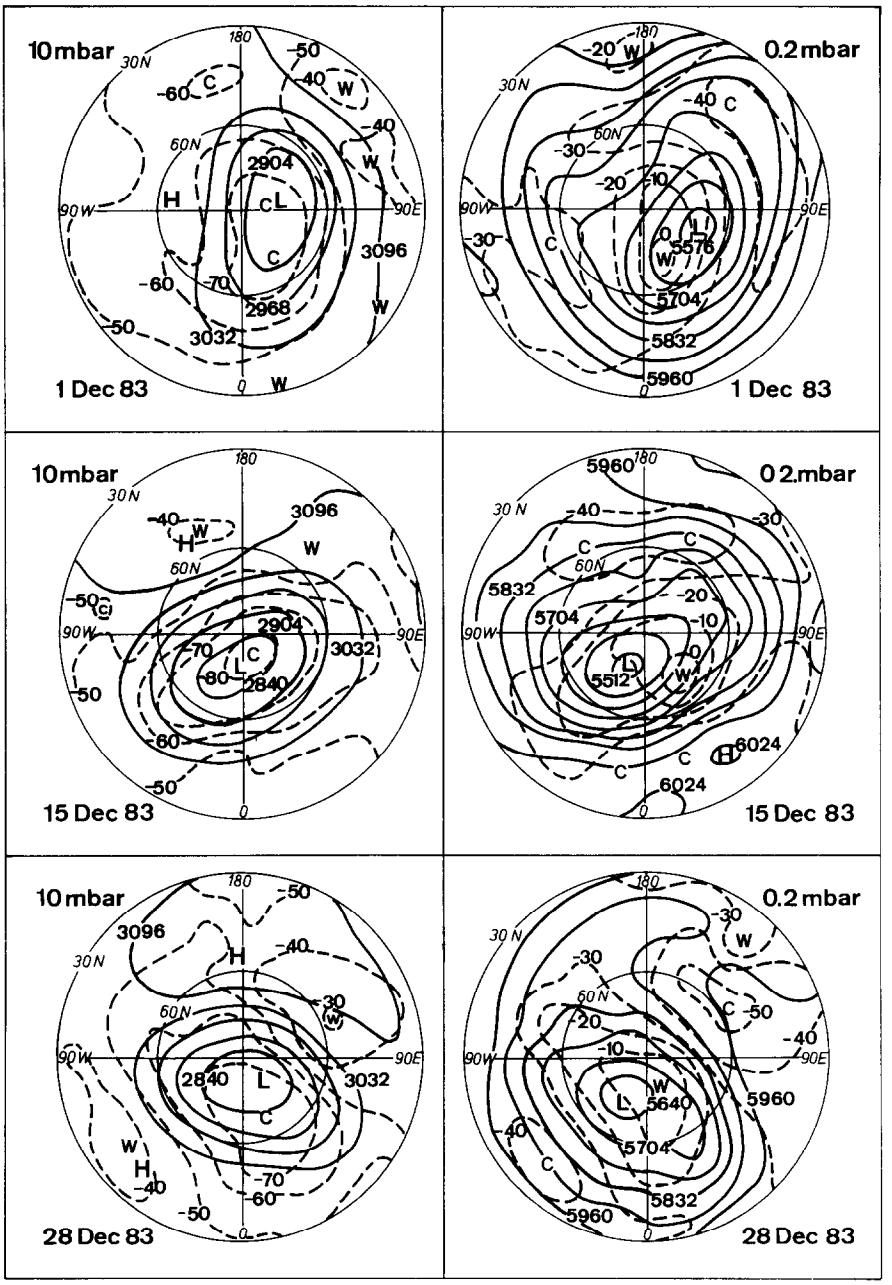

Fig. 2. Height (geopot. dm) and temperature (°C) maps. (a) Left 10 mbar level; right 0.2-mbar level. On 1 Dec. 1983, 15 Dec. 1983, 28 Dec. 1983, 12 Jan. 1984, 26 Jan. 1984 and 9 Feb. 1984. (*Continued over.*)

a very different latitudinal shape of the mean zonal wind.

(a) The distribution of the mean zonal wind in the meridional plane (Fig. 3a) shows a nearly normal midwinter condition for 15 December. In fact, the Canadian warming had weakened the jet in the stratosphere on 1 December, but the subtropical jet in the mesosphere was well developed during the first half of December. The corresponding zonal mean temperature in Fig. 3b displays the stratopause sloping from 0.2 mbar at the north pole to 1 mbar in tropical regions.

The first minor warming at the end of December weakened the zonal flow considerably. The jet was

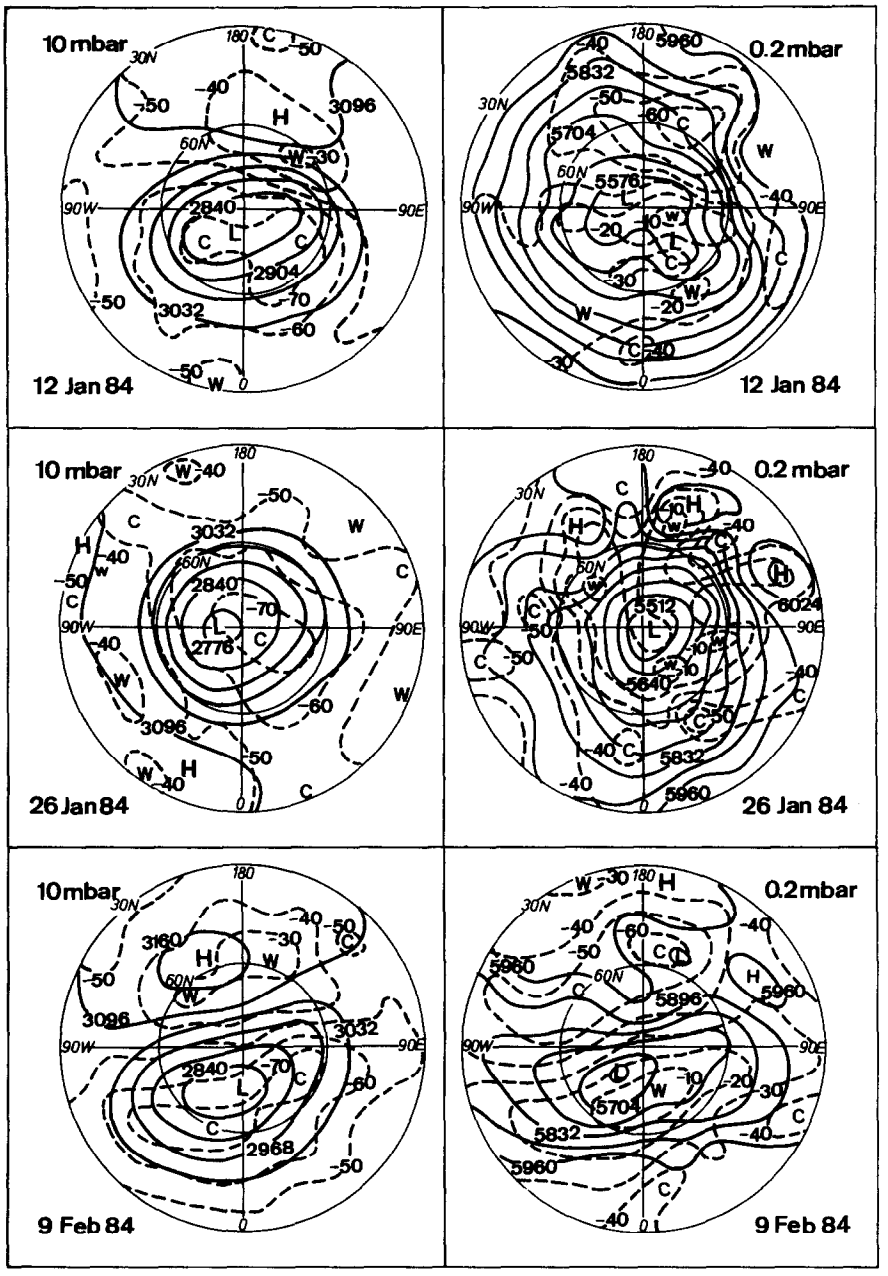

Fig. 2(a) continued.

split into two maxima, but the mesospheric jet was still placed at subtropical latitudes and a westerly mean flow governed the stratosphere north of 35°N and the lower mesosphere. Zonal mean temperatures at that time show warming at polar latitudes throughout the upper stratosphere. That this event is not a local phenomenon over northern Europe can be verified by the height–longitude sections in Fig. 5. Cooling in the mesosphere in mid-latitudes are connected with the decreasing mean zonal wind at 40–50°N.

(b) During January the zonal flow was re-established, but at the end of the month the jet maximum was situated at 60°N up to the mesosphere. This wind maximum at high latitudes is not a mean statistical feature, as recognizable from the long term mean for January (BARNETT and CORNEY, 1985), where the jet

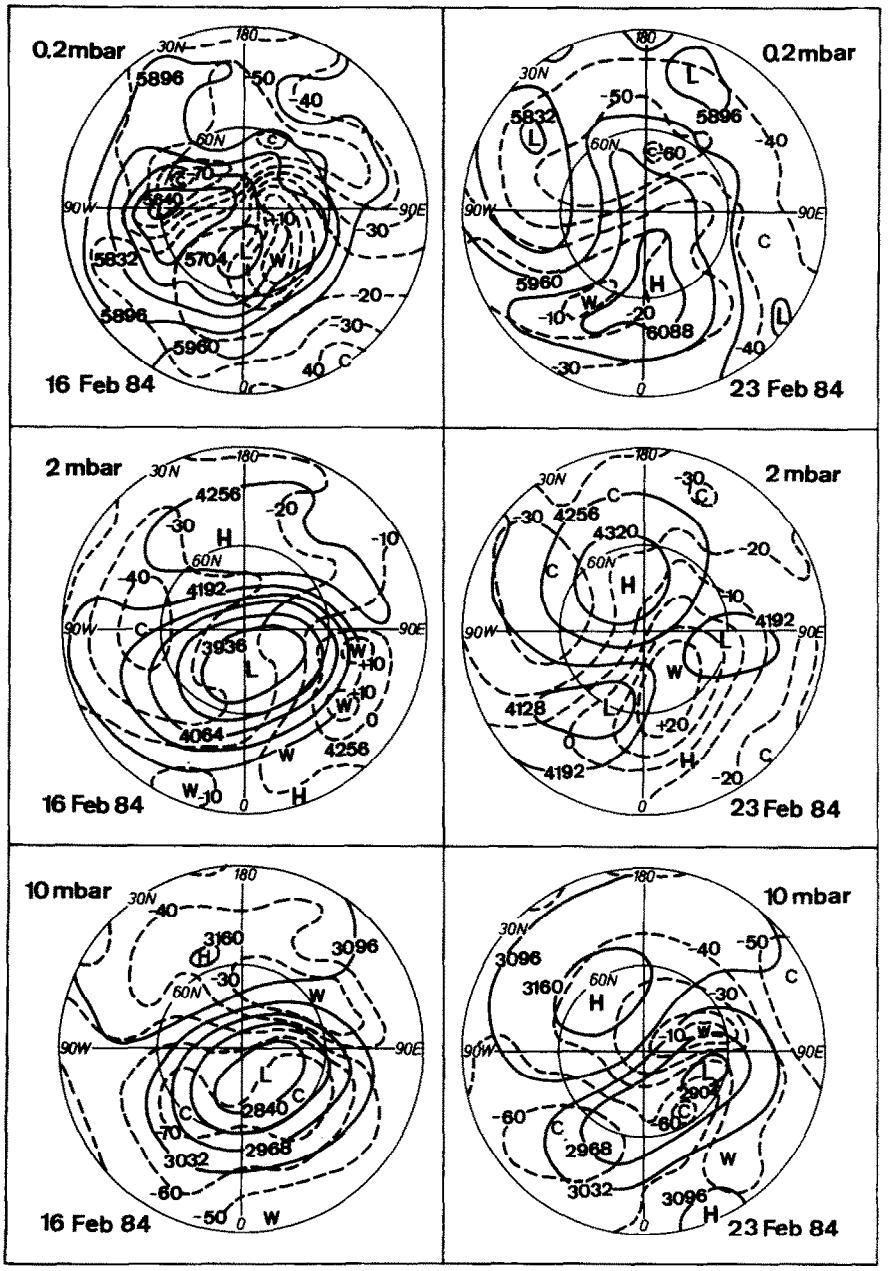

Fig. 2 continued. (b) Left 16 Feb. 1984, 0.2 mbar, 2 mbar, 10 mbar levels. Right 23 Feb. 1984, 0.2 mbar, 2 mbar, 10 mbar levels.

is strongly decreasing from December to January at all latitudes and heights. In January 1984 the strong meridional temperature gradient between the cold polar mesosphere and a warmer stratopause around 70°N is the reason for the jet maximum at high latitudes.

(c) By 9 February a pronounced change in the mean flow had started; the jet maximum at mid latitudes is weaker than at any time before in this winter and a stronger jet at tropical latitudes had developed. In the upper stratosphere only a weak jet at high latitudes is noticeable. The zonal mean temperature in Fig. 3b shows a relatively cold stratopause which lay uniformly over all latitudes around 1 mbar.

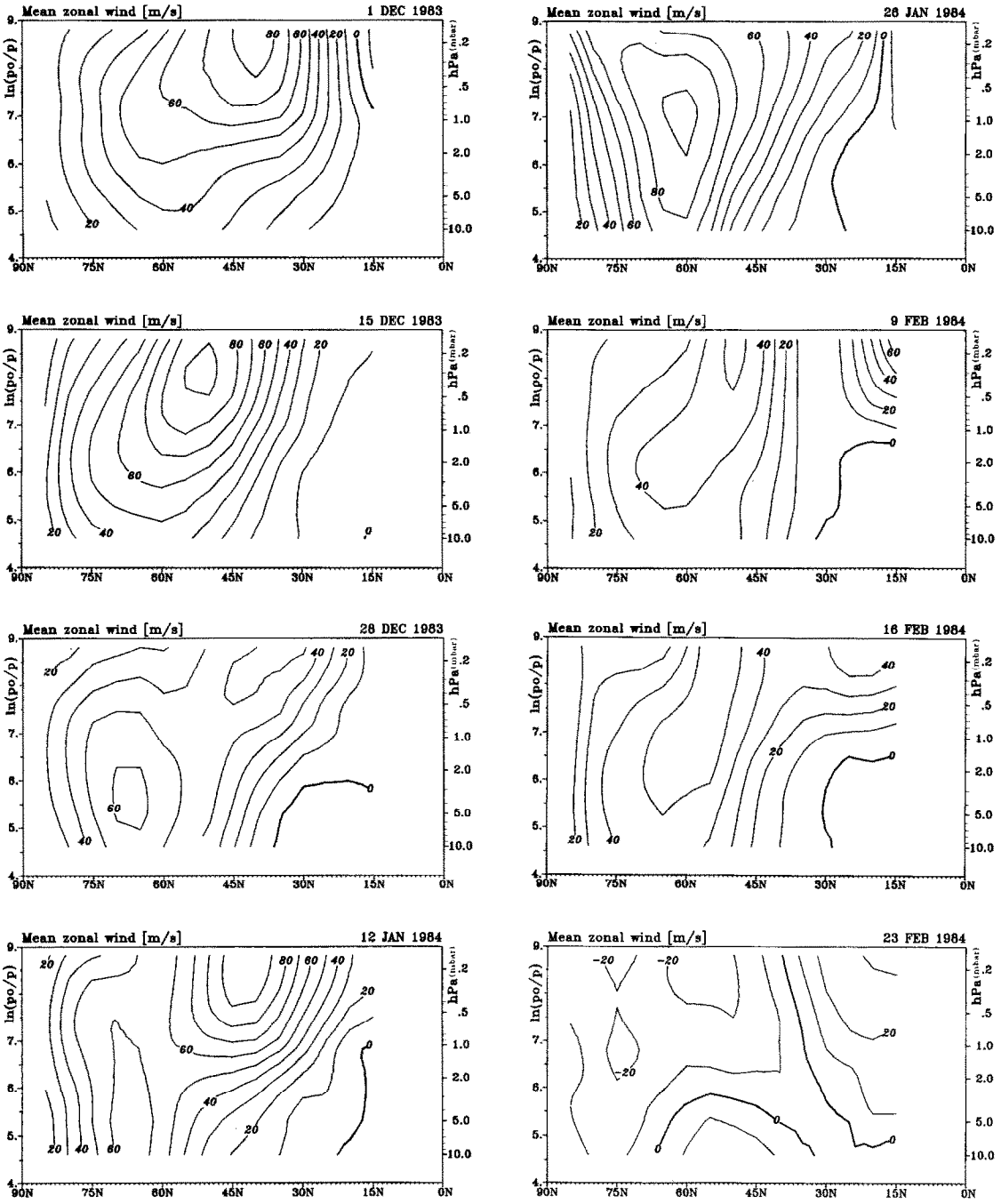

Fig. 3. Meridional cross-sections. (a) Zonal mean wind (m s^{-1}). (*Continued over.*)

The westerly zonal wind recovered slightly for a short time during February, but broke down completely afterwards within a few days, so that easterlies governed the whole stratosphere and mesosphere north of 60°N at the end of February.

The zonal mean temperature for the end of February in Fig. 3b indicates a very disturbed stratosphere and lower mesosphere; the stratopause region at high latitudes lies lower than the 1 mbar level and slopes upward to normal values in the subtropical and

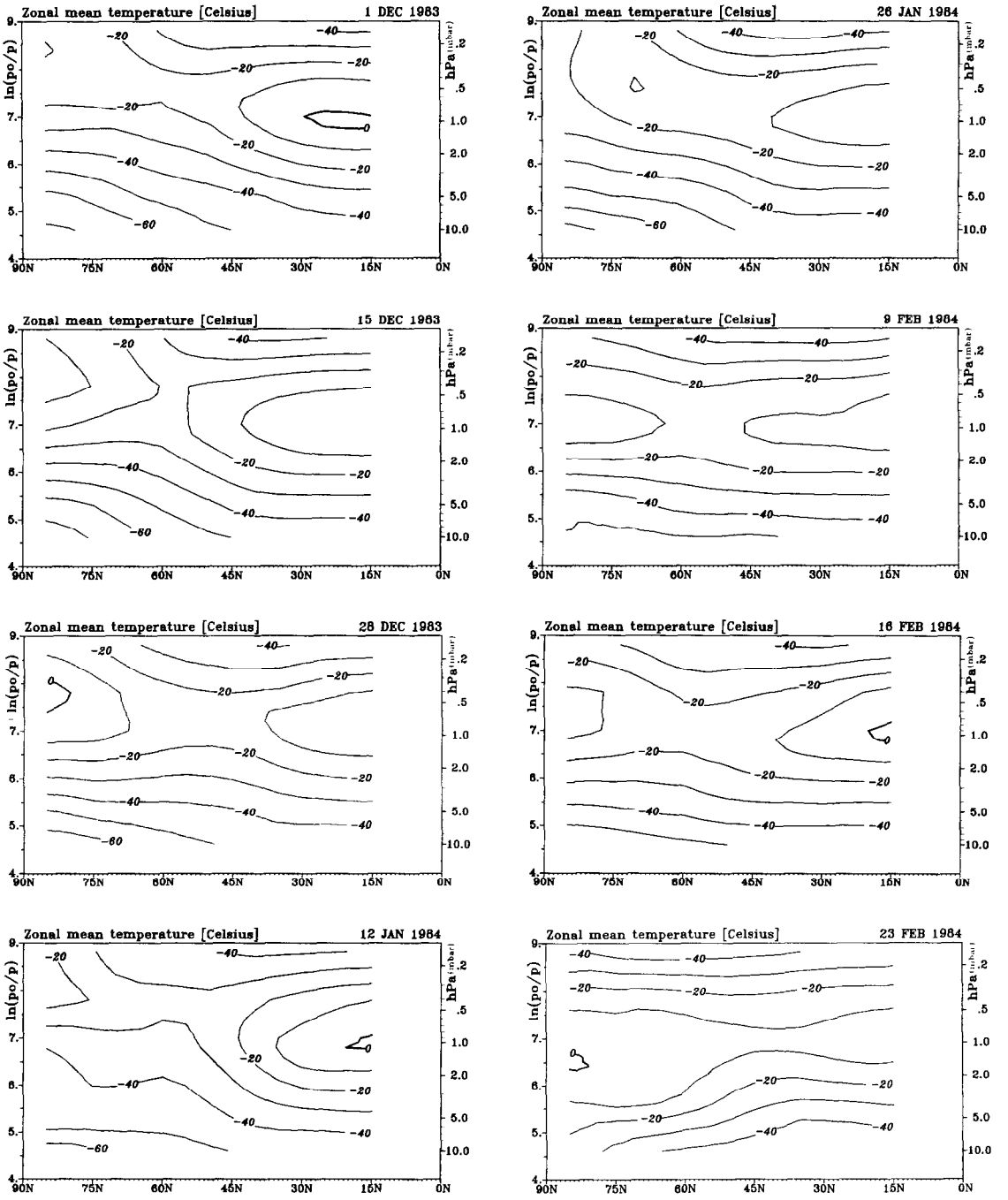

Fig. 3 continued. (b) Zonal mean temperature (°C).

tropical regions. Following the time series of the temperatures shown in Fig. 3b, a descent of the stratopause during the whole campaign period can be seen.

While the *zonal mean* of mesospheric temperatures over high and middle latitudes is considerably decreased only during the stratospheric warming, *local decreases* in mesospheric temperatures are also found during the minor warming at the end of December in Fig. 5a. Because of the phase of the temperature wave (zonal wavenumber one with max at 20°W), Andøya, Norway, is not really affected at

that time, showing only a slight temperature decrease at 60 km.

The longitudinal temperature sections at 40°N and 70°N for 23 February in Fig. 5a, b illustrate how the warm region sloped from a very high stratopause at 50°W, where the cold rest of the vortex (−65°C at 10 mbar) is situated, across the maximum near Andøya around 2 mbar to a warm region over Siberia with 0°C in the middle stratosphere. This lower part is well known from the analysed 10 mbar maps.

4.2. *Planetary waves*

The computed planetary wave amplitudes of wave number one and two for the geopotential height field (Fig. 4) show very clearly that the preferred domain of the first wave number is at high latitudes (60–70°N), whereas when wave number two is strong, it mostly acts at middle latitudes (45–50°N). It is well known that wave number one is commonly much stronger than wave number two, but in spite of the smaller amplitude the interaction with the mean zonal wind can be even larger for wave number two.

The time of the maximum amplitudes for wave one at high latitudes occurs when the polar vortex shifts to subpolar latitudes.

Growing amplitudes are connected with the processes leading to minor and major warmings, as seen on 28 December and 9–16 February.

The weakest amplitudes at the end of January are associated with a polar vortex centered at the north pole in the stratosphere.

In the mesosphere the vortex is strongly disturbed by wave number one at mid latitudes (see, for instance, in Fig. 2a at 0.2 mbar a trough over Europe and anticyclones over the northern Pacific on 26 January). The travelling part of wave one in the middle stratosphere could be followed by a daily series of height maps in the middle stratosphere. The period was nearly one month, as can be seen in a polar diagram for 30 mbar in LABITZKE *et al.* (1984). From middle January until 9 February wave one travelled westward, acting together with a standing wave one, which had its phase (max) over the Aleutian islands.

By 9 February a strong wave two had also developed (Fig. 4b), noticeable by the elongated polar vortex at 1 mbar (PETZOLDT, 1985). At that time the warm regions of eastern Asia and Europe at 1 mbar were already connected over the north pole, although it was 10 days before a northeastward moving warm pulse developing over low latitudes reached the polar area. For the middle stratosphere this process was described by the eastward moving wave one at 60°N from 9 to 17 February.

From 22 to 23 February the warm region crossed Andøya, Norway, from east to west and two rocket soundings of the MAP/WINE campaign measured maximum temperatures in the lowered stratopause. In Fig. 6 the temperature profiles are plotted, together with that of the SSU retrieval at the neighbouring gridpoint 70°N, 15°E for comparison.

5. DYNAMICAL RELATION BETWEEN LOW AND HIGH LATITUDES AND BETWEEN TROPOSPHERE, STRATOSPHERE AND MESOSPHERE

5.1. *Main features*

During the last few years theoretical work has given a new understanding of the processes which dominate the evolution of planetary waves and the mean flow in the stratosphere and mesosphere. It is well known that tropospheric waves propagate up to mesospheric heights and interact with the mean zonal flow. For planetary waves the so-called Eliassen–Palm vector (EPV) gives the propagation direction of the waves in the meridional plane (ANDREWS and MCINTYRE, 1976).

The horizontal component of the EPV is proportional to the negative eddy momentum flux and is given by $-\mathrm{A}\cos\varphi\,\overline{v'u'}$; the meridional component is the mean eddy heat flux divided by a static stability term and is given by

$$f\mathrm{A}\cos\varphi\overline{v'\theta'}\Big/\frac{\partial\bar{\theta}}{\partial p},$$

where u is the zonal wind component, v the meridional wind component, θ is the potential temperature and the prime denotes deviations from a zonal mean marked with an overbar (f is the Coriolis parameter, φ latitude and A radius of the Earth).

If this vector is divergent, the waves are feeding the westerly mean flow, i.e. a zonal force per unit mass is accelerating the westerly wind. If the EPV is convergent, a deceleration force is working on the westerly wind. Large meridional motions are forced by this wave–mean flow interaction in order to maintain geostrophy and mass continuity. The Coriolis torque and adiabatic motions connected with the forced meridional circulation are changing temperatures and winds in all involved layers.

The EPV shows clearly that not only do the eddies work on the mean zonal wind by their momentum transport, but also that the horizontal eddy heat flux is able to change the mean flow by its vertical divergence and the induced meridional motion. Accordingly, computations of the momentum divergence for

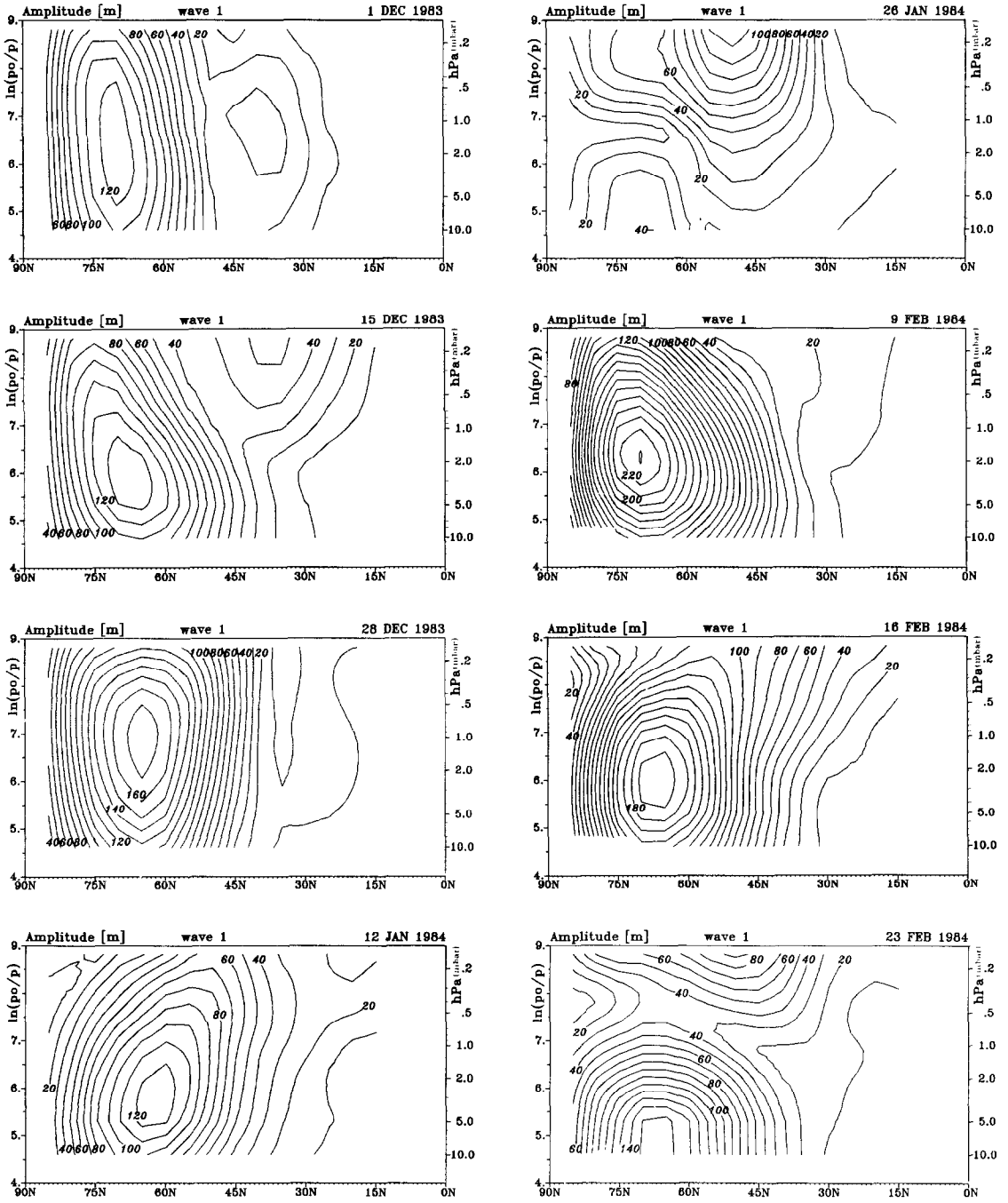

Fig. 4. Meridional cross-section of amplitudes. (a) Wave number 1 (geopot. dm). (*Continued over.*)

the MAP/WINE winter in the 20–25 km region by TARASENKO (1987) have shown that, even for this small layer, the sign of the wind change with time is not understandable only by eddy momentum transport. A careful temperature analysis is needed to compute the correlation product $\overline{v'\theta'}$ for the eddy heat flux.

Wave–wave interactions are also important, although they make the picture much more complicated, as do ageostrophic wind components and diabatic heating. The interpretation of successful simulations of stratospheric warmings (DUNKERTON *et al.*, 1981; BUTCHART *et al.*, 1982; ROSE, 1985) and the

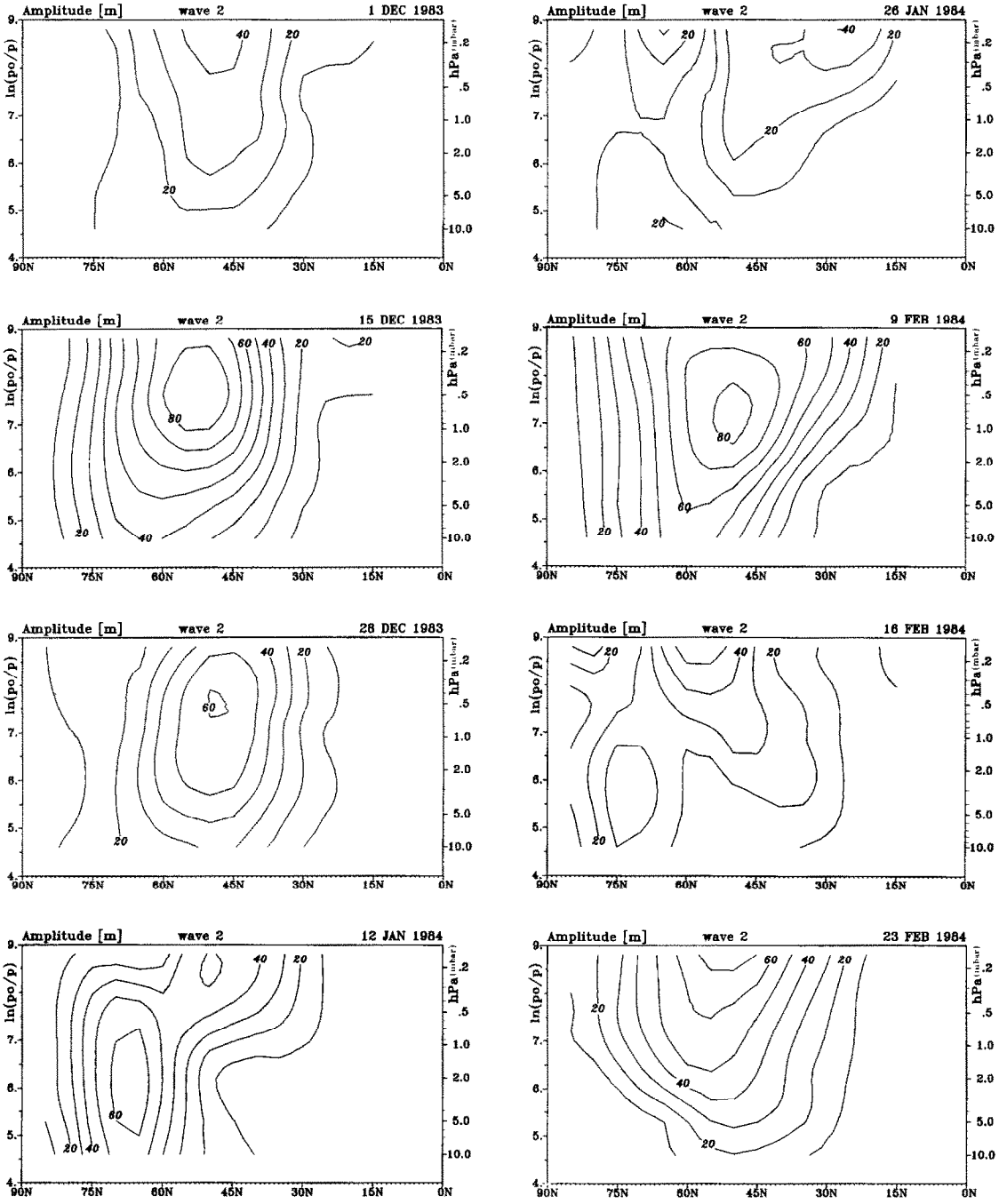

Fig. 4 continued. (b) Wave number 2 (geopot. dm).

careful analysis of valuable satellite data sets (SSU: PALMER, 1981; LIMS: GILLE *et al.*, 1984; SAMS: PETZOLDT *et al.*, 1986) shows that in principal these processes can be understood in the following way.

Normally, eddy energy is transported from the troposphere at middle latitudes upwards and towards the equator. In the winter stratosphere wave–mean flow interactions and wave–wave interactions give rise to fluctuating wave amplitudes at high latitudes. Eddy transports are changed by these fluctuations and sometimes wave energy is focussed into the polar cap in the middle atmosphere. Mostly this happens several

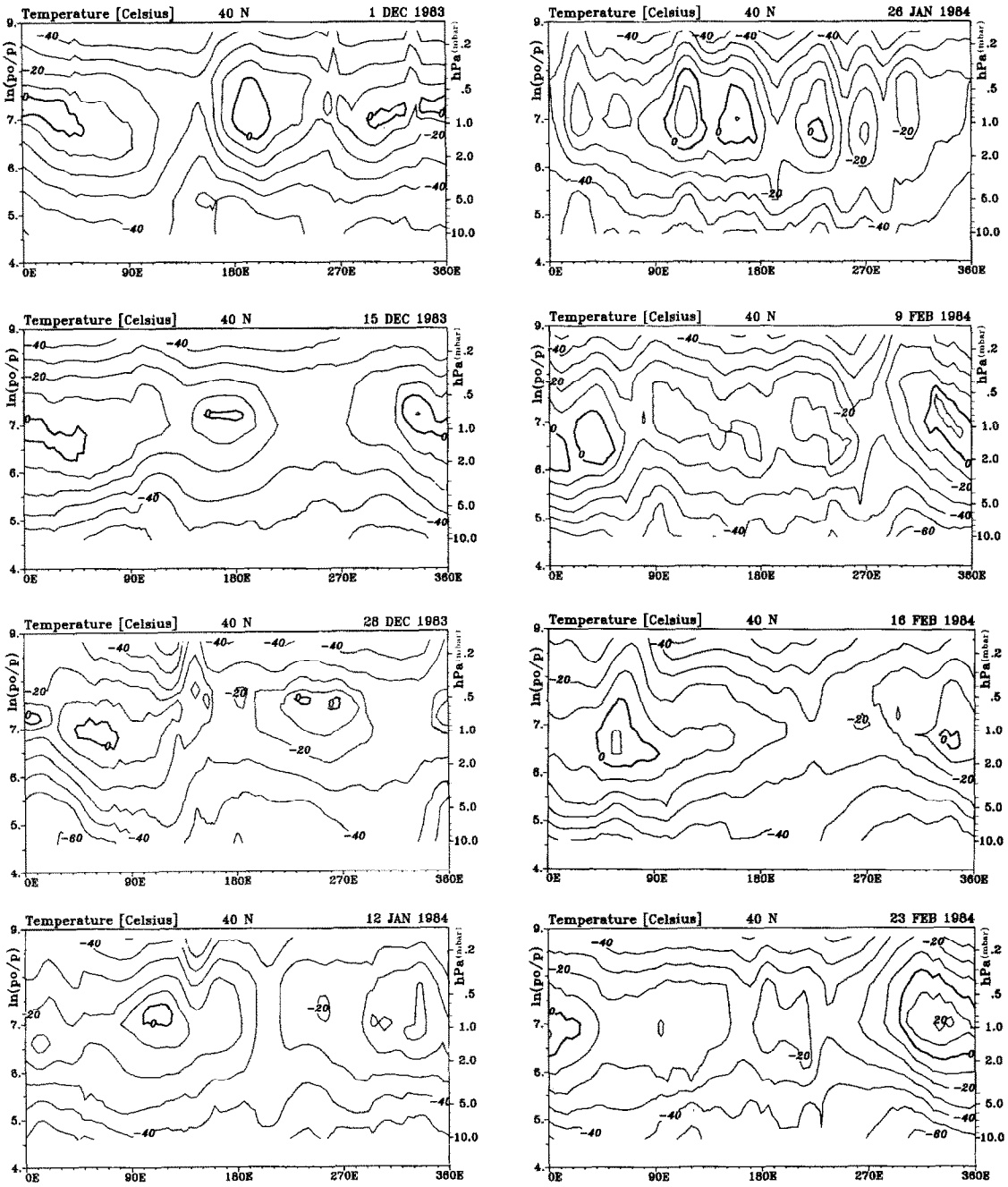

Fig. 5. Height–longitude sections of temperature (°C). (a) 40°N. (*Continued over.*)

times a winter, until suddenly the westerly zonal flow is broken down by strongly northward focused wave energy up to the stratopause.

5.2. *Open questions*

The analysis of the MAP/WINE data set points out the fact that in addition to the main features of the circulation which were previously known, more detailed investigations are necessary for an understanding of the dyamical coupling between the processes.

Open questions are:

(a) why and when do wave-like disturbances develop at the high stratopause;

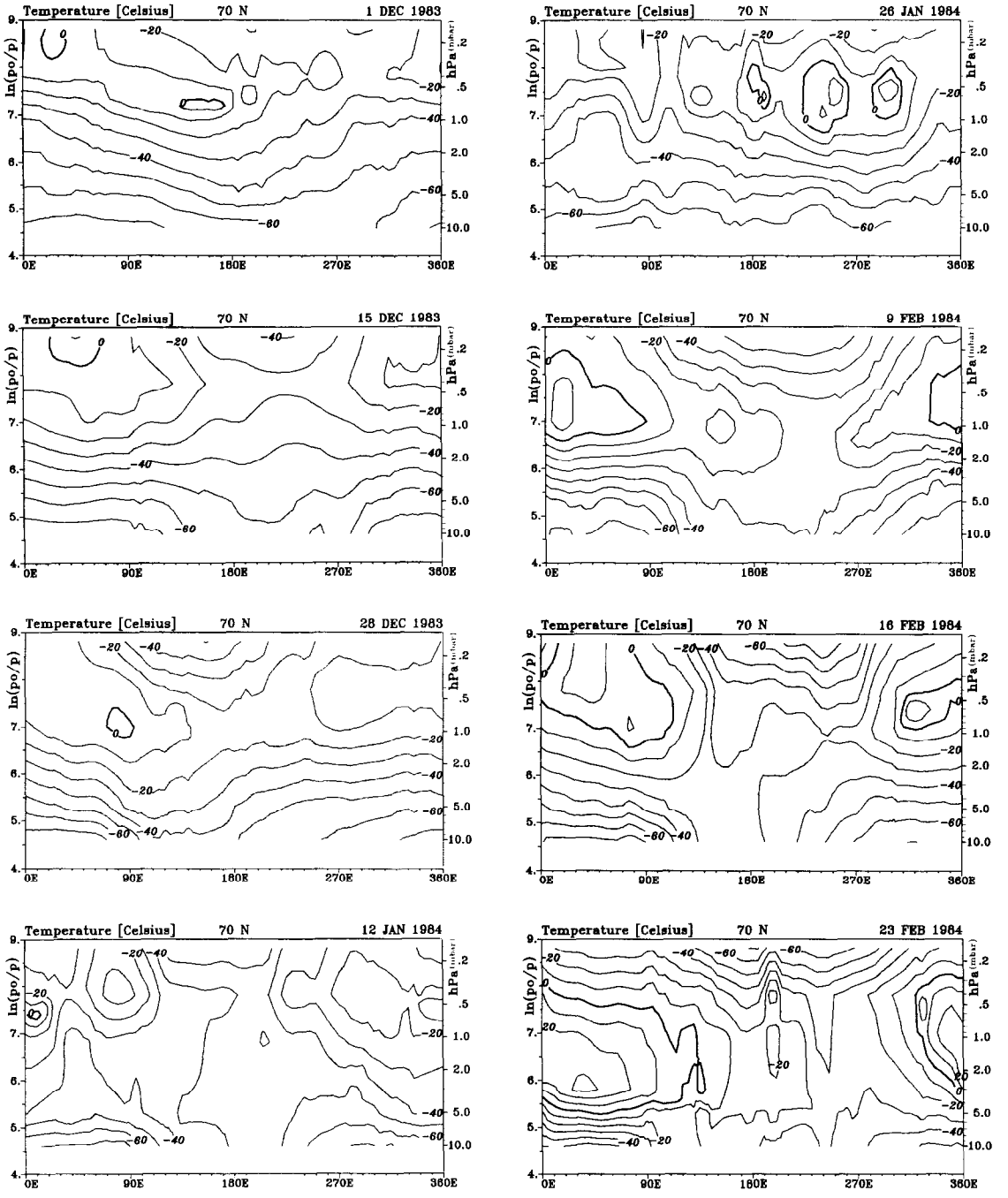

Fig. 5 continued. (b) 70°N.

(b) why and when will these disturbances turn into a major warming;

(c) does the decrease of the large scale vertical wavelength, shown by the sinking stratopause and mesopause, influence the height range where gravity waves deposit their momentum by breaking;

(d) which processes are responsible for the amplification of smaller horizontal wavelengths during a warming;

(e) is the description in terms of *zonal waves* suitable for the warm events extending from low latitudes and explosively producing very steep lapse rates

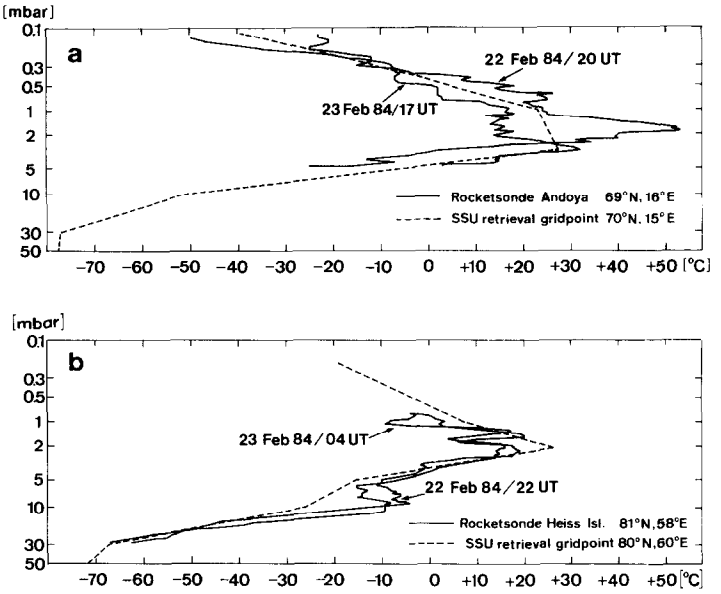

Fig. 6. Temperature profiles on 23 Feb. 1984 from rocketsondes and retrieved from SSU radiances. (a) Andøya, 69°N, 16°E. (b) Heiss Island, 81°N, 58°E.

and horizontal temperature gradients, like frontal zones;

(f) how are these disturbances reproduced above the mesopause?

A contribution to the second part of question (a) could be given in Section 4. For the answer to question (b) a suggestion from a former work using SAMS data (PETZOLDT *et al.*, 1986) is supported qualitatively by the MAP/WINE data in the following Section, 5.3, and will be treated quantitatively in a forthcomming paper. Question (c) could be treated by cooperation of several experimenters during this campaign and should be continued as a second step in MAC (Middle Atmosphere Cooperation). Breaking waves or non-linear wave–wave interaction could be the answer to question (d), but to arrive at a decision by computing the enstrophy balance of the waves from real data would be very difficult, as mostly the balance cannot be closed. Some insight should be possible from the enstrophy balance during a simulated warming in a spectral model. For question (e) some work has to be done with a frontogenetic scheme. A tentative answer to question (f) is given in LABITZKE *et al.* (1987).

5.3. *Dynamical conditions for the breakdown of the zonal mean flow*

A reversed meridional gradient of the potential vorticity seems to be a sufficient condition for the breakdown of the westerly flow around the polar vortex, when wave activity there is reflected at a critical wind layer back towards the polar region, as theoretically pointed out by WARN and WARN (1978). A critical wind line in the meridional plane is reached when the phase speed of the waves equals the mean flow velocity.

It can be shown with SAMS data for the winter 1979/1980 (PETZOLDT *et al.*, 1986) that the southward eddy transport of potential vorticity in the center of the mostly convergent EPV led, during several weeks, to an increase of potential vorticity at subtropical latitudes. At the same time, the fluctuating potential vorticity at higher latitudes reached low values, so that the meridional gradient became zero.

A critical wind line reaching from subtropical to middle latitudes at that time led to a breakdown of the zonal flow by convergence of the partially northward reflected planetary wave activity (see Fig. 7b).

The same seems to be true for the breakdown during February 1984. As long as there is no critical wind line the upward propagated fluctuating waves are working at the mean flow of the polar vortex, but the main wave activity is led equatorwards (as shown for 1980 in Fig. 7a). Even the strong minor warming at the end of December did not bring a breakdown of the flow. The reason is that in the mesosphere the jet maximum in subtropical regions (Fig. 3a) is still

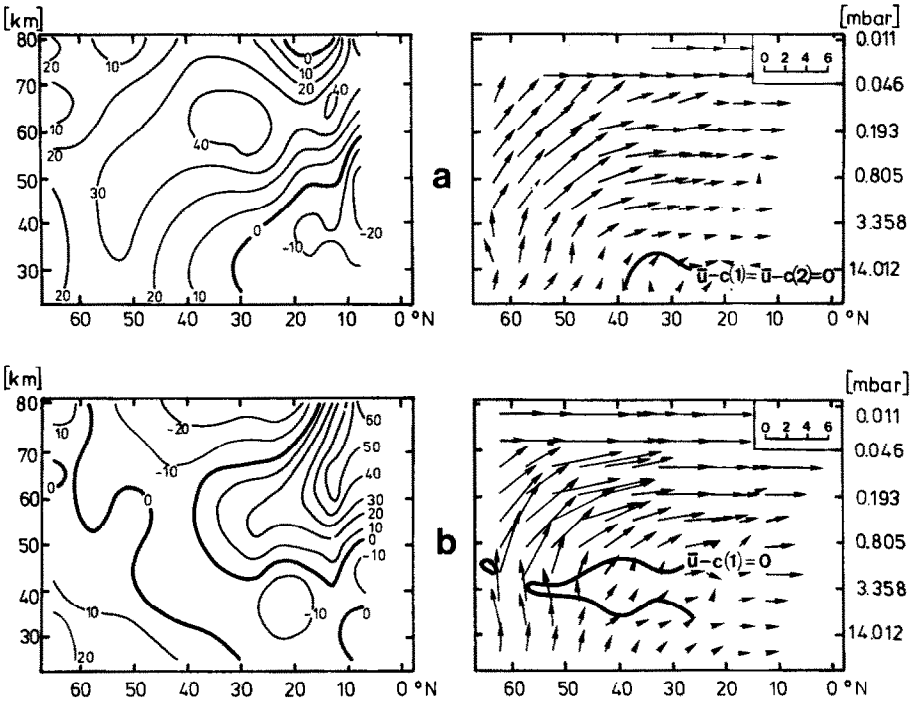

Fig. 7. Meridional cross-sections of mean zonal wind (m s^{-1}) (left side) and EPV (right side) (horizontal scale at top right in 10E14 kg m s^{-1}, vertical scale to be multiplied by 5.5E−3). (a) 23 Feb. 1980. (b) 27 Feb. 1980. From PETZOLDT and SCHOLL (1986).

responsible for the southward transport of wave activity, though in the lower stratosphere some northward wave refraction might have taken place. This northward focusing of wave activity—as shown by a poleward directed EPV—is often observed in the middle stratosphere during the winter (see for instance the negative centers of momentum transport in LABITZKE *et al.* (1984) for the 30 and 50 mbar levels). This seems to be connected with the 16 day wave (MADDEN *et al.*, 1981).

A conclusion about when this focusing is efficient enough to displace the vortex from the polar area and to establish an easterly flow from 60°N to the pole can only be made with a knowledge of mesospheric dynamics. The wave disturbances at the end of December 1983 and in the first half of February 1984 were comparable, but only at the end of February did a breakdown occur, presumably because then the necessary conditions (deceleration of the mesospheric jet by strong wave activity) *and* the sufficient conditions (reversed meridional gradient of the potential vorticity at a critical wind layer) were fulfilled. The cut-off at subtropical latitudes of the mesospheric wind maximum on 9 February provided the first occurrence of a critical wind layer. For the eastward moving wave one (see Section 4.2) the isotach of 10 m s^{-1} near 40°N in Fig. 3a is a critical wind line.

However, the zonal flow recovered slowly during the next week. Therefore whether the vorticity gradient at that time was already reversed must be investigated.

It is expected that the reversal of the meridional gradient of the potential vorticity was first achieved at the next step of deceleration after 16 February, when the rapid development of the major warming indicates the reflection of wave activity to higher latitudes.

Acknowledgement—Financial support by the Deutsche Forschungsgemeinschaft for this project under grant no. 372/13-3 is very much appreciated. Also, the technical assistance of the stratospheric research group of Prof. KARIN LABITZKE is gratefully acknowledged. Thanks for the technical preparation of all figures are due to B. EHMKE.

REFERENCES

Andrews D. G. and McIntyre M. E.	1976	*J. atmos. Sci.* **33,** 2031.
Barnett J. J. and Corney M.	1985	*Handbook for MAP* **16,** 47.
Butchart N., Clough S. A., Palmer T. N. and Trevelyan P. J.	1982	*Q. J. R. met. Soc.* **108,** 475.
Dunkerton T., Hsu C.-P. F. and McIntyre M. E.	1981	*J. atmos. Sci.* **38,** 819.
Gille J. C., Bailey P. L. and Beck S. A.	1984	*J. geophys. Res.* **89,** 711.
Gille J. C. and Lyjak L. V.	1984	*AEPS: Dynamics of the Middle Atmosphere* (Holton J. R. and Matsuno T., Eds) p. 289. Terra Scientific Publishing Company.
Labitzke K., Naujokat B., Lenschow R. and Petzoldt K.	1984	*Beil. Berl. WettKarte* **SO 15/84**
Labitzke K., Manson A. H., Muller H. G., Rapoport Z. and Williams E. R.	1987	*J. atmos. terr. Phys.* **49,** 639.
Leviton R.	1975	Final Report WMO-No. 395.
Madden R. A.	1978	*J. atmos. Sci.* **35,** 1605.
Matsuno T.	1970	*J. atmos. Sci.* **28,** 1479.
Offermann, D., Gerndt R., Küchler R., Baker K., Pendleton W. R., Meyer W., von Zahn U., Philbrick C. R. and Schmidlin F. J.	1987	*J. atmos. terr. Phys.* **49,** 655.
Nash J. and Brownscombe J. L.	1983	*Adv. Space Res.* **2,** 59.
Palmer T. N.	1981	*J. geophys. Res.* **86,** 9679.
Petzoldt K.	1979	*Remote Sounding of the Atmosphere from Space*, p. 89. Pergamon Press, Oxford.
Petzoldt K.	1980	*Met. Abh. Inst. Met. Berl.* Ser. A **2,** 1.
Petzoldt K.	1985	*Proceedings of the 7th ESA Symposium on European Rocket and Balloon Programmes and Related Research*, p. 33. ESA SP-229.
Petzoldt K. and Scholl M.	1986	*Beitr. Phys. Atmos.* **59,** 301.
Rose K.	1985	*Beitr. Phys. Atmos.* **58,** 220.
Rush D. W., Mount G. H., Zawodny J. M., Barth C. A., Rottmann G. J., Thomas R. J., Thomas G. E., Sanders R. W. and Lawrence G. M.	1983	*Geophys. Res. Lett.* **10,** 261.
Warn T. and Warn H.	1978	*Stud. appl. Math.* **59,** 37.

Reference is also made to the following unpublished material:

Tarasenko D. A.	1987	Personal communication.